
# Proposed Thermal Camera Monitoring System for Preventative Maintenance of Electrical Apparatus

Prepared by Mason Field

# Memo of Transmittal

Date: April 14, 2020

To: Dallas Chubey and Sulayman Bah

From: Mason Field

Subject: Results for Proposed Thermal Camera Monitoring System

---

I hope to have done justice to a topic that requires further research. This report is an entry into a chronic inquiry for a thermal camera system that can be used to monitor and log the thermal signatures of electrical apparatus with intent to elicit useful information from logged data. Project authorization was inferred from January's class conversations.

The report was primarily limited by equipment restrictions and safety considerations. Due to COVID-19 lab time was not available, and equipment could not be used to properly simulate faulty apparatus. A toaster oven with adjustable temperature was adequate for simple thermal tests.

Background research was conducted to understand the nature of blackbody radiation due to its fundamental relationship with thermal radiation/infrared spectrum radiation; additionally, known electrical heat loss theory was included to highlight the relationship between thermal radiation and electrical heat losses.

Research into thermal detector technology was conducted to understand the nature of thermal radiation detection; further, emphasis was placed on thermopile arrays because they are used in the proposed system. Optical systems were covered briefly to understand the materials used in thermal radiation detection. Reliability engineering and data analysis methods were researched to understand a method with which to analyze collected data. The thermal camera system was researched in two parts, as hardware and software, because both required different degrees of research and both are self-contained systems in and of themselves. The case study confirmed that a thermal camera system can be developed for low cost and have many useful applications.

Conclusions:

1. All electrical systems produce power losses in the form of heat which can damage system apparatus.
2. All objects above zero kelvin radiate infrared spectrum energy.
3. All infrared radiation can be detected with an infrared detector.
4. A thermal camera system can be used to monitor and log equipment temperature.
5. Apparatus temperature can be analyzed to create metrics for proper operation and aberrant operation.
6. Equipment temperature metrics can be used as benchmarks for system health; primarily, to determine proper and aberrant operation of apparatus.
7. Advanced metrics can be used for sophisticated system/apparatus health.

Recommendations:

1. Determine a list of suspect apparatus.
2. Begin monitoring suspect apparatus with thermal camera system.
3. Create metrics for proper and aberrant operation of apparatus.
4. Set alarms for apparatus that surpass tolerance limits of metric.
5. Investigate applications for advanced data analysis metrics and system wide nodal analysis metrics.

This report is a brief and unexhaustive glance at a topic that requires proper development. With the availability of low-cost thermal arrays and increasingly connected networks of devices (5G) there are no financial or physical limitations to implement useful monitoring systems; therefore, research and development of these systems should continue beyond the scope and limitations of this report. For questions or concerns regarding this report please contact Mason Field by phone [(306)380-4347] or email [Field5300@saskpolytech.ca].

# PROPOSED THERMAL CAMERA MONITORING SYSTEM

## FOR PREVENTATIVE MAINTENANCE OF ELECTRICAL APPARATUS

Presented to Dallas Chubey and Sulayman Bah of Saskatchewan Polytechnic

Prepared by Mason Field

April 14, 2020

# Executive Summary

Research indicated that a system could be used to monitor and log the thermal signatures of electrical apparatus and elicit useful system information from thermal data to avoid system failures; therefore, a thermal camera system was proposed, designed, and tested.

Background research was conducted to understand the relationship between blackbody radiation and electrical heat losses, and the financial significance of the thermal camera system. Research was conducted to understand infrared detectors, infrared optics, reliability engineering and preventative maintenance, the thermal camera system design, and advanced system metrics. Primary Research was a case study that showcased the ability of the proposed thermal camera system to record thermal signatures and process data into useful preventative information.

The following conclusion and recommendations are based on the research and case study performed for the report; where, conclusions are what were learned or proved in the report and recommendations are the suggested actions justified by the conclusions.

Conclusions:

1. All electrical systems produce power losses in the form of heat which can damage system apparatus.
2. All objects above zero kelvin radiate infrared spectrum energy.
3. All infrared radiation can be detected with an infrared detector.
4. A thermal camera system can be used to monitor and log equipment temperature.
5. Apparatus temperature can be analyzed to create metrics for proper operation and aberrant operation.
6. Equipment temperature metrics can be used as benchmarks for system health; primarily, to determine proper and aberrant operation of apparatus.
7. Advanced metrics can be used for sophisticated system/apparatus health.

Recommendations:

1. Determine a list of suspect apparatus.
2. Begin monitoring suspect apparatus with thermal camera system.
3. Create metrics for proper and aberrant operation of apparatus.
4. Set alarms for apparatus that surpass tolerance limits of metric.
5. Investigate applications for advanced data analysis metrics and system wide nodal analysis metrics.

# Table of Contents

# Table of Illustrations

# List of Formulas

# 1.0 Introduction

## 1.1 Background

### 1.1.1 Infrared Detection History

In 1800 William Herschel used coloured filters to help limit the transmittance of the sun through his telescope; interestingly, he noticed that the heat he felt on his eye depended on the colour of filter he used [1][2]. Herschel's experiments that followed concluded that certain monochromatic wavelengths near the end of the red spectrum relate to heat [1][2]. J. Seebeck had discovered in 1821 that a change in temperature of two dissimilar conductors generated a voltage at their junction [3][4], and by 1833 Italian physicists Leopoldo Nobili and Macedonio Melloni had already developed the first thermocouple and thermopile, respectively [3][4][5]. These Italian inventions, namely the thermopile, allow for sensitive measurements of heat or infrared spectrum electromagnetic radiation [3][4]. The bolometer was invented by S.P. Langley in 1881 and was designed to outperform the contemporary thermopiles [6]. A biased bridge circuit was used to measure the resulting net current from two detector elements whose resistance would change with infrared absorption [3][4]. Refer to Appendix A for a detailed timeline of Infrared technology advancements.

### 1.1.2 Blackbody Radiation

All electromagnetic waves propagate as a spectrum of varying wavelengths, refer to the macro and micro wavelength spectrum in Figure 1. Any object above absolute zero kelvin will radiate heat primarily in the infrared spectrum wavelengths [4] and follow established physical relationships.

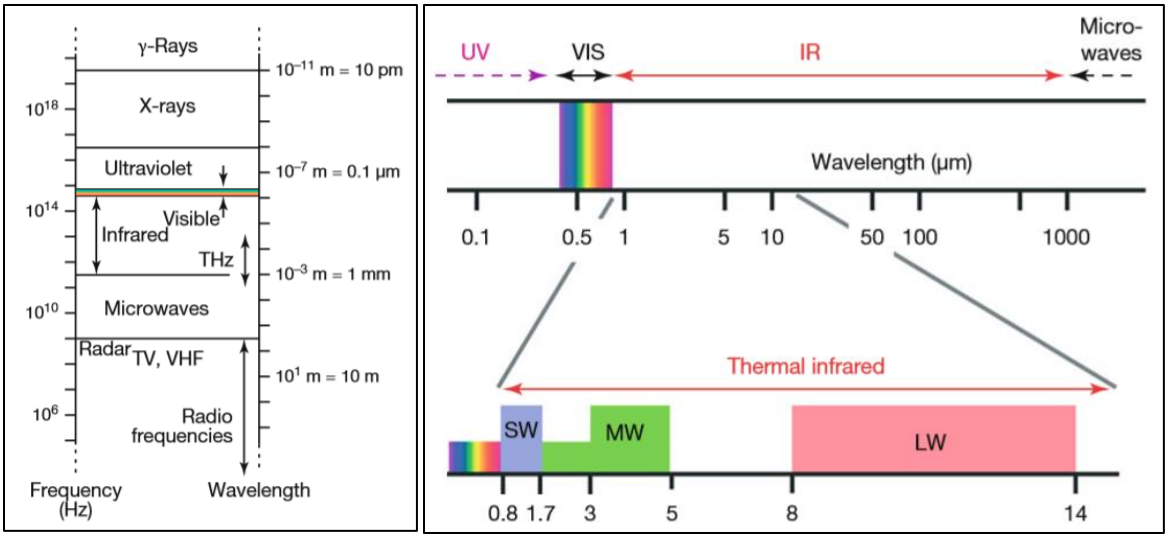


*Figure 1: Electromagnetic Spectrum Macro and Micro View [4]*

The foundation for infrared spectrum electromagnetic radiation can be elicited from the following formulas. Planck's law (the first instance of a quantum equation [4][7]) is the most significant in scope, interpretation and application because it includes the speed of light and Plank's constant; further, the derivative and integral of Planck's Law is Wien's Displacement law and Stefan-Boltzmann Law, respectively. Figure 2 is a plot of Planck's law at multiples of temperature plotted with Wien's law superimposed. Wien's law is the maxima of the curve and Stefan-Boltzmann Law is the area under each curve. Refer to Appendix B for the derivation of Wien's Law and Appendix C for the derivation of Stefan-Boltzmann Law from Planck's Law.

#### *1.1.2.1 Kirchhoff's Radiation Law*

Kirchhoff's Radiation Law is defined as; Where $\varepsilon\lambda$ is the emitted radiation and $\alpha\lambda$ is the absorbed radiation.

$$I\lambda = \frac{\varepsilon\lambda}{\alpha\lambda}$$

[3][4][6][7][8]

*1.1.2.2 Stefan-Boltzmann Law*

Stefan-Boltzmann Law for blackbodies is the total energy radiated from an object and is defined as

$$P = \sigma A T^4$$

[3][4][6][7][8]

For objects with a certain emissivity absorbing or radiating net power defined as

$$P = \sigma \varepsilon A (T^4 - T_e^4)$$

$$\sigma = 5.67 * 10^{(-8)} \frac{\mathrm{W}}{\mathrm{m}^2\ \mathrm{K}^4}$$

[3][4][6][7][8]

*1.1.2.3* Wien's Displacement Law

Wien's Displacement law is defined as the product of the maximal wavelength at a temperature and the product of the max wavelength and temperature is constant defined as

$$\lambda_{max} T = 2.898 K \mu m$$

[3][4][6][7][8]

*1.1.2.4* Planck's Law

Planck's Law for energy distribution of a blackbody is defined as

$$I(\lambda) = \frac{2\pi h c^2}{\lambda^5} * \frac{1}{e^{\left(\frac{hc}{k\lambda T}\right)} - 1}$$

$$Where\ k = 1.38 * 10^{-23} \frac{J}{k}\ and\ h = 6.626x10^{-34} J * s$$

$$units\ work\ out\ to \frac{irradiance}{\lambda}$$

[3][4][6][7][8]

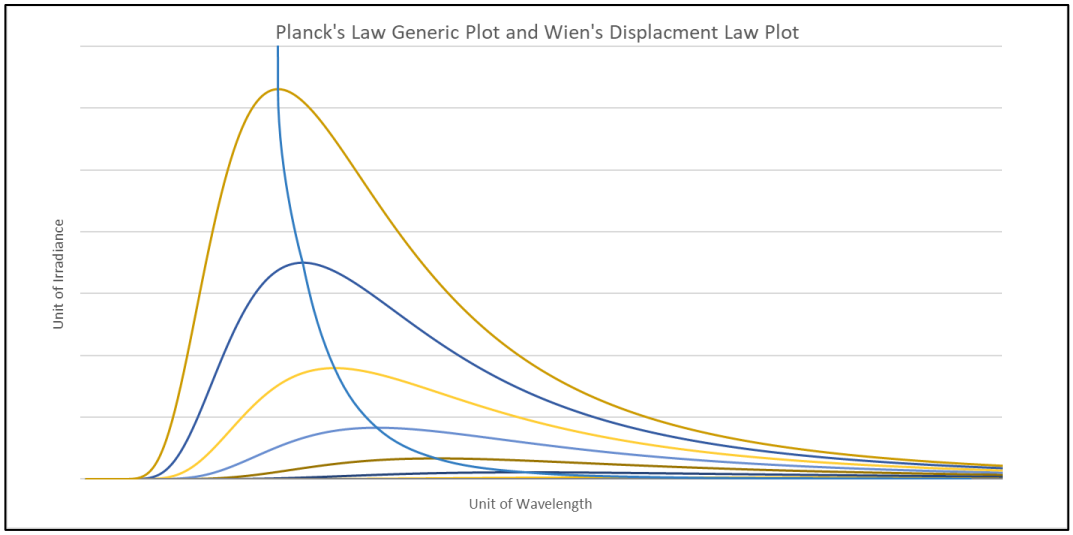


*Figure 2: Planck's Law and Wien's Displacement Law Curve Plot*

### 1.1.3 Electrical Heat Radiation

Power losses are radiated as heat in electrical systems; therefore, the related formulas are examined here. Combinations of these formulas can be used to solve for information in the electrical system. See Appendix D for an example of electrical formulas and blackbody radiation formulas used together to solve electrical variables.

#### *1.1.3.1 Current Formula*

Current is the rate of charge flowing in a material defined as

$$I = \frac{Q}{t}$$

[9]

#### *1.1.3.2 Resistance Formula*

Resistance is the opposition to current flow in the material defined as

$$R = \rho \frac{l}{A} (1 + a20\,\Delta T)$$

[9]

#### *1.1.3.3 Heat Loss Formulas*

Heat losses are generated when current flows through resistance and is defined as

$$P = I^2R$$

[9]

or in rotating electrical machines generate and radiate heat losses at points of friction defined as

$$P = 1.05 * 10^{-4} M * n$$

[10]

## 1.2 Purpose

The purpose of this paper is to introduce a method of preventive maintenance in an electrical system by using thermal imaging to collect data, and data extrapolation to create useful metrics; specifically, on medium and low voltage systems.

All electrical systems produce heat losses by electrical resistance and mechanical friction. When an aberrant electrical or mechanical condition exists, these systems operate and radiate heat levels above their nominal rating. When systems are operated above their nominal heat rating, they begin to degrade, and without corrective maintenance the equipment will fail.

Heat is associated with radiation of infrared spectrum wavelengths; therefore, their propagation, absorption and emission will be analyzed and applied to understand the function of devices used to detect heat in nominal and aberrant electrical systems. Metrics for preventative maintenance of equipment can be deduced from the data collected by the monitoring devices; therefore, data collection and analysis methods will be analyzed and applied to mathematic models to create metrics that can aid in preventative maintenance.

## 1.3 Significance

Thermal imaging is significant because it can be used to identify aberrant conditions that could cause a loss of service; furthermore, the thermal imaging database system proposed in this paper can collect the data required to create metrics that can contribute to diagnosing the health of the electrical system while remaining low in cost and maintenance.

All sectors of society that require electricity to function are susceptible to loss of electrical service, this downtime has a spectrum of negative effects defined on the x and y-axis as importance and urgency, respectively; naturally, safety and economy are the primary maxima. A 2013 paper by Y. Yoshida and R. Matsuhashi found an average cost of a one-hour outage across Japanese industry as $672¥\frac{kW}{h}$[10]; therefore, for a customer with 1000kW load, an average outage would cost $8681CAD per hour and creates sufficient budget headroom to implement a thermal monitoring system.

## 1.4 Scope

- Analysis of photon and thermal style infrared detectors and infrared optical materials.
- Analysis of reliability engineering specific to preventative maintenance.
- Description of proposed thermal camera system.
- Basic analysis of collected thermal data from thermal camera system.

## 1.5 Limitations

- Lab access not possible due to COVID-19 which limited experiment sophistication.

## 1.6 Research Methods

Research was split into primary and secondary sources.

1. Primary sources
    - Calculations
    - Plots
    - Experiments
    - Designs
2. Secondary Sources
    - Textbooks
    - Journals
    - Government Standards
    - Datasheets

## 1.7 Key Terms

Thermography, Data Analysis, Preventative maintenance, Raspberry Pi, MLX90640

# 2.0 Discussion of Findings

## 2.1 Infrared Detectors

Infrared detectors can be categorized into photon and thermal detectors [3][4][8]. Photon detectors work by measuring the change in a material's electrical properties when photon absorption causes a change in charge carrier state in the material [3][4][8]. Thermal detectors work by measuring the change in an electrical variable in the detector material when there is a change in the material temperature [3][4][8]. Photon detectors are not used in this report due to availability and cost but further information on them is included as a comparison to thermal detectors.

### 2.1.1 Photon Detectors

Photon detectors function by converting photon energy absorbed in a material into released electrons, where the energy required to shift a charge carrier from the valence band to the conduction band is defined by the bandgap of the material and measured in electron volts [3][4][8]. The electrical properties of the material vary proportionately with the change in charge carrier state; therefore, the variance in electrical properties of the material can be measured to determine the total photon irradiance [3][4][8]. This method requires a wavelength to accommodate a large enough charge to change charge carrier states in the material; consequently, the wavelengths that photon detectors can detect are limited to a specific band or must be cooled [3][8]. Photon detectors are also known as quantum detectors because their founding principle is the measurement of individual photon energy; therefore, Planck's constant and probability are utilized to model the incident radiation power [3][4][8].

### 2.1.2 Thermal Detectors

Thermal detectors function by absorbing infrared radiation and varying the temperature of the detector material [3][4][8]. If the material has an electrical variable that is proportional to a change in temperature then a change in temperature of the material will cause a change in the electrical variable

of the material; therefore, the change in the electrical variable can be measured[3][4][8]. The primary influence in thermal detectors is the absorbed temperature; therefore, a larger range of wavelengths can be measured compared to photon detectors [3][4][8]. Thermal detectors are further categorized by their construction, which are numerous, refer to Appendix E for a list of popular thermal detectors and their method of operation.

*2.1.2.1 Thermocouple, Thermopile and, Thermopile Arrays*

The thermoelectrical principles that thermocouples follow were pioneered by J. Seebeck in 1821 [3] when he observed that a potential difference is found at the junction between two dissimilar conductors when there is a change in their temperatures; Expressed in $\frac{uV}{K}$. Figure 3 shows the initial design that Seebeck used to observe the voltage generation of the thermocouple.

$$\Delta V = \alpha_s \Delta T$$

[3]

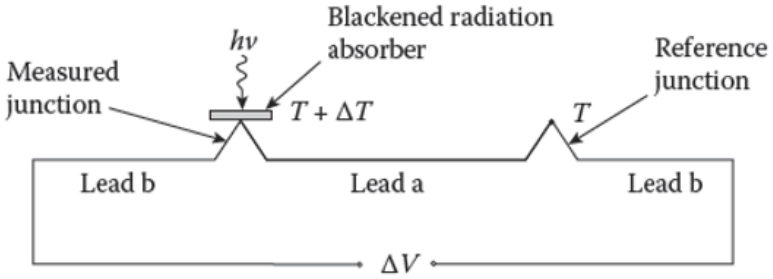


*Figure 3: J. Seebeck Thermocouple Schematic [3]*

The output of a thermocouple is measured in uV/K and Nobili noticed it is too small for practical measurements [5]. The thermocouple creates a potential from the thermoelectrical response from two dissimilar conductors; therefore, the pile can be placed in series to create a larger potential and a larger measurable value [3][4][8]. This series configuration of thermocouples is called a thermopile and its design is credited to Melloni [5]; Figure 4 displays the connection of a thermopile. Coefficients for the

dissimilar conductors are notated as $\alpha_a$ and $\alpha_b$ and their difference equals $\alpha_s$; Therefore, a thermopile's change in potential is defined by

$$\Delta V = N(\alpha_a - \alpha_b)\Delta T$$

[3]

Where $N$ is the number of thermocouples in the thermopile.

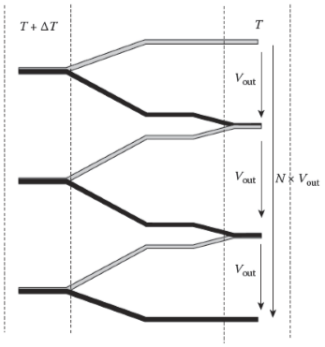


*Figure 4: Series Connection of Thermocouple as Thermopile Schematic [3]*

The Thomson and Peltier effects counter the Seebeck effect which produces the potential between the two conductors [3][8]. The Peltier effect is equivalent to counter emf and the Thomson effect explains the relationship between heat conduction gradients and current flow in a conductor [3][8]. Both countereffects should be taken into consideration when designing a thermopile. If the reader requires a detailed mathematical analysis of the Thomson and Peltier effects find them in Thermal Infrared Sensors by H. Budzier and G. Gerlach [8].

Modern era thermopiles can be produced with semiconductor materials and utilize integrated chip manufacturing (micro-machining) to reduce size, cost and allow for the design of thermopile arrays [3][4][8]. A detector array is simply many detectors arranged so that many points of detection are available, and a final image can be formed from these points. Each detector makes up one pixel in an array [3][4][8]. The MLX90640 thermal sensor used in this report is an example of a 24x32 thermopile array; the array layout can be seen in Appendix F. A detailed teardown of the MLX90640 sensor is available for $4489 [12] from Research and Markets online store; unfortunately, there was only a $100

budget allocated for this report. In place of a proper teardown see Figure 5 which is a typical single micro-machined detector, this detector is one of 756 elements that make up the MLX90640's 24x32 detector array.

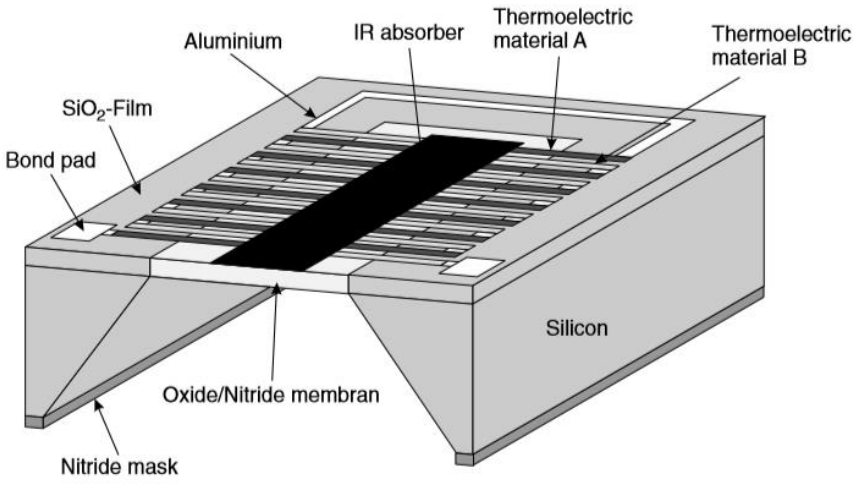


*Figure 5: Micro-machined Thermopile Detector [8]*

### *2.1.2.2 Bolometer, Micro-bolometer and Micro-bolometer Arrays.*

S. P. Langley published *The Bolometer and Radiant Energy* in 1881, wherein he set out to develop a device that would measure quantities of radiant heat with equal accuracy and greater sensitivity than the contemporary thermopiles [6], which had dominated the field since their inception in 1833 [3][4][8]. The design uses a current source to bias a Wheatstone bridge circuit that is connected to the sensing element of the bolometer. The bolometer has two sides that are constructed identically with wires spaced in channels across the surface. When one side of the bolometer element is exposed to a radiating source the resistance of the wire changes and results in a difference of currents in the Wheatstone bridge circuit which can be measured. The measurements from Langley's bolometer exceeded his goals for accuracy and sensitivity as the error was less than one percent (1/10000 of a Celsius change caused noticeable deflections in the galvanometer), and 10 to 30 times more sensitive

than thermopiles [6]; Additionally, his bolometer responded to changes in temperature quicker due to the wire in the bolometer having a small thermal capacity and large temperature coefficient [6]. The original design and test results by Langley can be seen in Appendix G.

Modern bolometer research was initiated by United State Military contracts given to Honeywell and Texas Instruments in the 1980s [8]. The information was made public in 1992 [8] and applied integrated circuit (IC) processing technology to produce bolometer arrays at a low cost, and high volume [3][4][8]. Refer to Appendix H to see a cross-section of a modern bolometer array.

## 2.2 Infrared Optics

Infrared detectors require an optical system to gather and focus infrared radiation onto the detector. Everyday optics such as eyeglasses, camera lenses, projector lenses and similar systems are designed to augment the radiation that is visible to the human eye [13]; therefore, optical systems that augment the visible light spectrum transmit visible light spectrum radiation and are not designed for radiation outside of the visible spectrum. Infrared spectrum radiation is outside of the visible light spectrum; therefore, visible light spectrum optical systems should not, and in many cases cannot be used to augment infrared radiation [3]. Refer to Appendix I where the transmission spectrums of optical materials are shown.

For example on a sunny day, a child is outside at a picnic table playing with a magnifying glass, they notice the visible light from the sun can be concentrated when the magnifying glass is positioned a certain distance away from the table creating a strong point where all the rays meet on the table. After a couple of attempts, the child was able to keep the rays focused on one point to produce smoke and a burn mark. The resulting radiating energy required to create this burn mark is primarily from visible light, this is because solar radiation is roughly emitting radiation at a temperature of 5250C; therefore, the irradiance is greatest between 400nm – 800nm and the magnifying glass can focus this spectrum of energy efficiently. Wien's Law can be used to find the wavelength where infrared radiation is maximum;

$$\lambda_{max}T = 2.898K\mu m \therefore \lambda_{max} = \frac{2.898K\mu m}{5250+273.15K} = 524.70nm$$

Refer to Figure 6 to see the irradiance spectrum that the child would be playing with on a clear sunny day and that peak irradiance is at ~524.70nm. But what if solar radiation was emitted at 100C? The energy contained in these photons would be primarily in the far infrared spectrum at

$$\lambda_{max}T = 2.898K\mu m \therefore \lambda_{max} = \frac{2.898K\mu m}{100+273.15K} = 7766.31nm$$

This radiation could not be focused by the child's magnifying glass because the magnifying glass material does not transmit energy beyond 2000-3000nm, assuming crown glass is used [4][14]. In this case, the child would need a magnifying glass that is designed with materials that have high transmittance of infrared spectrum radiation (visible light is no different than infrared *light* it is simply travelling at a different wavelength). Infrared optics are all designed with the transmittance of infrared spectrum wavelengths, most materials are opaque and utilize coatings to reduce imperfections [3][4][8].

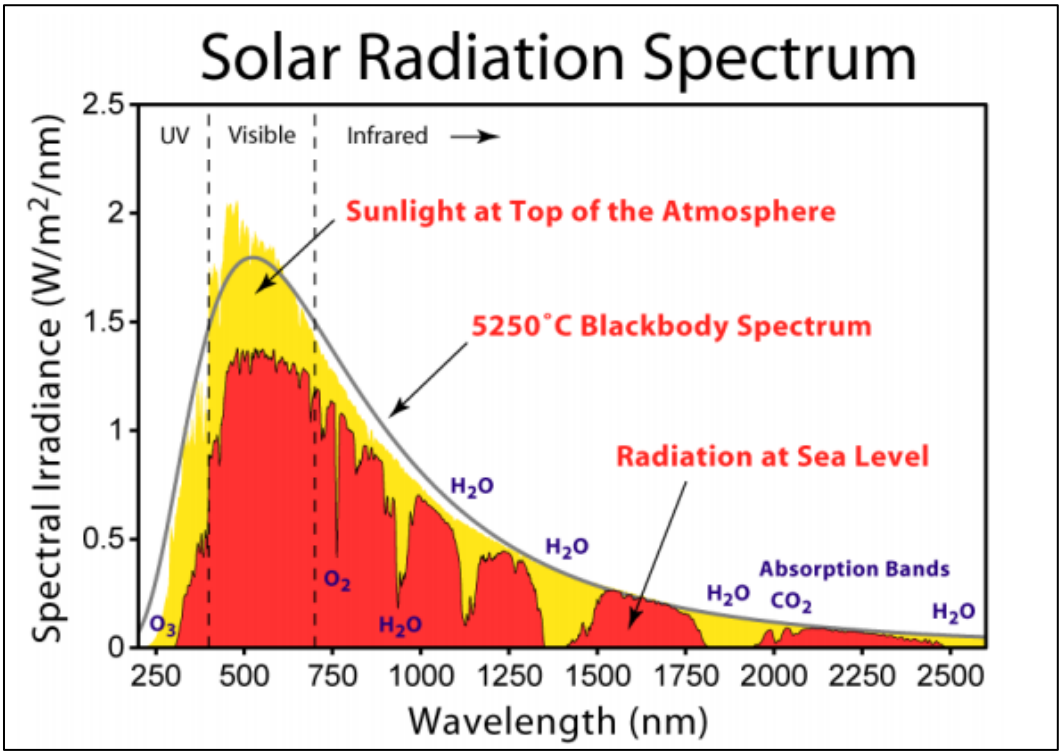


*Figure 6: Solar Radiation Irradiance over Wavelength Plot [33]*

## 2.3 Reliability Engineering and Preventative Maintenance

Because of the wide scope that reliability engineering encompasses (refer to Appendix J for work scope figure) this paper considers Alessandro Birolini's Reliability Engineering [15] as the de facto standard in reliability engineer; therefore, "The purpose of reliability engineering is to develop methods and tools to evaluate and demonstrate reliability, maintainability, availability, and safety of components, equipment, and systems" [15]. Reliability, affordability, maintainability, availability, and safety are the primary criteria that reliability engineers assess when developing methods to protect an asset [15][16][17]. Electrical maintenance can be divided into corrective maintenance and preventative maintenance; where, corrective maintenance is conducted after failure and preventative maintenance is conducted prior to failure [7]. NASA's Reliability-centered Maintenance Guide explains that preventative maintenance functions on the principle that failure probabilities can be found statistically [16]. In this report analysis of the temperature datasets allow for metrics to be created that precede failure probabilities, but these metrics over time would allow for failure probabilities to be found such as in a system like the United States Army's Failure Modes, Effects and Criticality Analyses system (FMECA) [17].

### 2.3.1 Electrical Equipment Tolerances

Specific electrical equipment tolerances are dependent on the equipment being inspected; consequently, the generic tolerance table from ANSI/NETA should be used as a guideline only and not as a substitute for manufacturer datasheets [18]. Refer to Appendix K for the NETA Thermal Testing Standards Table. When possible a thermal analysis for specific apparatus should be conducted to determine site-specific tolerances. For example, any aluminum apparatus is more susceptible to thermal raise impact than copper apparatus [19]. Due to coppers higher thermal capacity, 0.98 versus 0.48, it can dissipate heat more efficiently than aluminum [19] and because resistance increases with a change in temperature [Formula 1.1.3.2] there exists a state of positive feedback that increases the dissipated

heat; empirically, this increase in resistance relationship can be observed in thermal fuse time curves and can explain why apparatus tends to burn up exponentially, rather than linearly, with respect to time.

## 2.4 Proposed A.S.H. Thermal Camera System

A Small Helpful (ASH) Thermal Camera System was made with hardware and software that monitors the thermal signatures of electrical and mechanical apparatus in an electrical system and logs preconfigured temperature ranges into a database, hosted on the system, that can be accessed and analyzed for patterns that correlate with the electrical system's health.

### 2.4.1 Proposed A.S.H. Infrared System Hardware

Three generic components are required for the proposed system, a single board computer, a thermal sensor, and an HMI display. Specifically, a Raspberry Pi 3B+, Melexis MLX 90640 110° FOV Thermal Sensor, and Adafruit TFTPI 240x240 Display were selected for their availability and low cost. See Figure 7 for the wiring diagram of the three components, and datasheets for all hardware are available upon request.

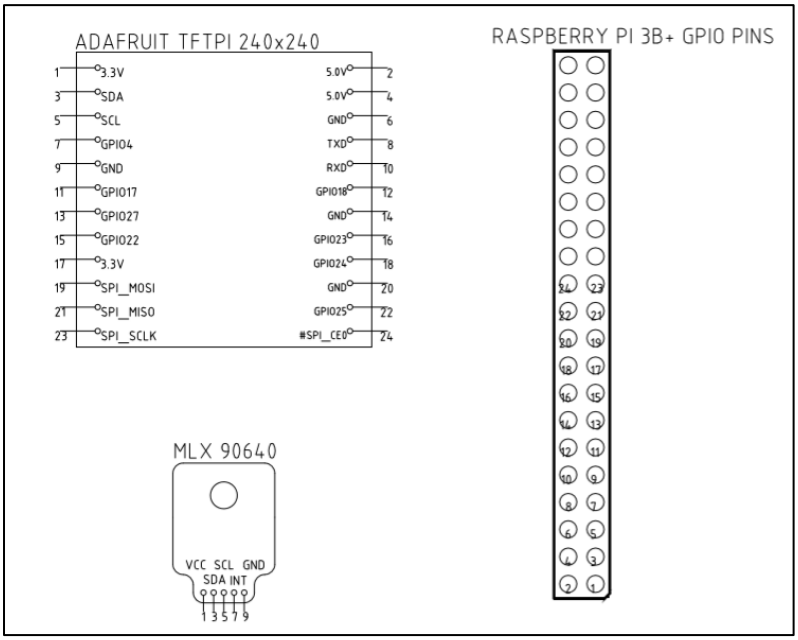


*Figure 7: Wiring Diagram for Components of Thermal Camera System*

#### *2.4.1.1 Single Board Computer*

A single-board computer is a typical generic PC miniaturized to fit onto a single palm-sized Printable Circuit Board (PCB), while it maintains many of the functions of a normal PC it sacrifices power and sophistication for size and affordability [20]. Because of their size, affordability and flexibility the single board computer can be thought of as a general development platform for this design, the Raspberry Pi is the monkey wrench in a metaphorical tool kit, it is not the right fit but it fits nonetheless.

The Raspberry Pi Zero W has the required, GPIO pins to interface with the MLX 90640 and TFTPI 240x240 display, WiFi 2.4GHZ module to connect wirelessly to networks for access, and processing power to host the software required for the database and data processing [20].

#### *2.4.1.2 Thermal Sensor*

Thermal sensors detect the irradiance of infrared radiation from an object with an array of detectors then display the array as pixels to form an image, thermal sensors were discussed in depth in Section 2.1.2.1.

The MLX 90640 is a 24x34 thermopile array, each thermopile detector makes up a single pixel in the 768 that make up the entire image [21]. Refer to Appendix E to see a readout of the MLX90640's thermopile array.

#### *2.4.1.3 HMI Display*

A Human Machine Interface (HMI) allows the end-user to communicate with the thermal camera system in the field to retrieve data and send orders. This design primarily used the HMI to display the thermal sensor data as a video stream.

The Adafruit TFTPI 240x240 display was purchased carelessly and is not recommended due to its 1:1 aspect display ratio that is at odds with the 3:2 aspect ratio of the thermal camera's 32x24 detector array, this results in a cropped 3:2 output on the 1:1 display or scaled 3:2 output on the 1:1 display. It is recommended that a 3:2 ratio display is used.

### 2.4.2 Proposed A.S.H. Infrared System Software

An A.M.P (Apache, MySQL, and PHP) software combination is required. Apache, MySQL and PHP are a web server, database server and programming language, respectively. These are required to host a web server where the local database can be accessed and manipulated with the programming language [22]. Figure 8 is a process flow chart for how the system interacts. The cloud bubble rectangles represent software components and solid rectangle outlines represent hardware components.

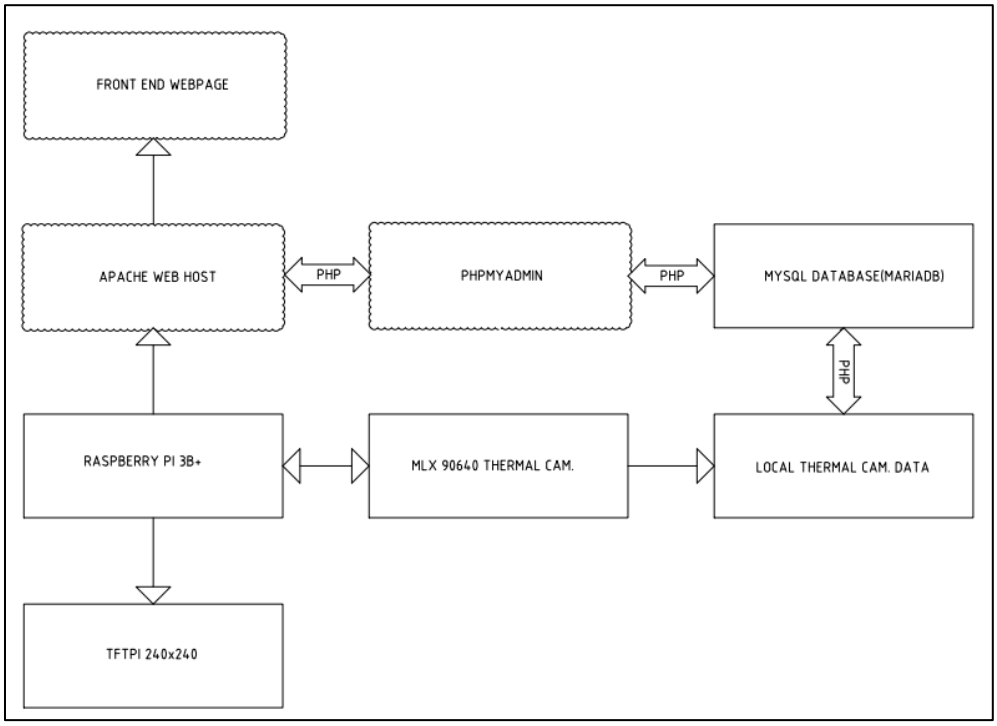


*Figure 8: Process Flow Diagram for Thermal Camera System*

#### *2.4.2.1 Web Server Client-server Model*

A web server allows for the files on a physical system to be interfaced on a network, the network can be an intranet or internet [22][23]. The web server takes requests from devices and then serves that content to the device in a web browser. HTTP (Hypertext Transfer Protocol) is the protocol used by webservers to transfer data [22][23]. A web server allows for the data on the Raspberry Pi to be

accessed on other devices on the same network and is required for users to access PHPmyAdmin which configures the database software.

Apache is used because it is free, the most used web server software available and, can be installed on the Raspberry Pi's Linux based operating system [22]. There are 20+ other webservers available, some open source, and some proprietary that could be used interchangeably for this project [24].

#### *2.4.2.2 Database client-server*

Database server software provides database services to other programs and computers following the client-server model [22]. The database server is like the web server but instead of files, database entries are requested and served [22]. A database server is required to organize and store the data from the thermal sensor**.**

MySQL is used as the database server hosted on the Raspberry Pi because it is open source and has been used in many applications with large volumes of data [22]. A non-exhaustive list of companies that utilize MySQL for database services includes Netflix, YouTube, Spotify, Twitter, Tesla, and NASA because of its flexibility and applicability [25].

#### *2.4.2.3 Programming Language*

A programming language is used to interface with hardware and instructs what actions are processed. PHP is used in this instance to communicate between the web server and the database server [22]. PHPmyAdmin is hosted on the webserver and acts as a graphical user interface to interact with the MySQL database.

### 2.4.3 Thermal Camera Cost Analysis and Feasibility

The Pimoroni MLX90640 sensor is $77.85 [26], the Raspberry Pi Zero W is $13.41 [27] and the PiTFT 1.3" screen is $20.33 [28] for a total of $111.59 exceeding the $100 budget by $11.59. The cost could be reduced by sourcing the MLX90640 sensor in bulk where 500 units are $63.42ea. [29], and

replacing the PiTFT 1.3” display with a generic TFT display for $11.43 [30] to reduce the total cost of the design to $88.26. No direct cost comparison can be made because there are no commercial contemporaries to the proposed thermal camera system, but NASA documented average rental rates in 2008 for a thermographic system was $2000CAD per week and a thermographic contractor was $1400CAD per day [16]. FLIR currently rents thermal systems for 10% of MRSP per week [31]. The proposed thermal camera system is feasible, and implementation would not be limited by any existing industrial or commercial maintenance budget. (Note: The Raspberry Pi 3B+ could not be sourced so the Raspberry Pi Zero W was quoted instead.)

## 2.5 Thermal Camera System Case Study

A piece of “electrical apparatus”, a toaster oven, was monitored by the thermal camera system where nominal and aberrant thermal signatures were captured and compared for correlating metrics between the two signatures. Pearson’s correlation coefficient and a definite integral were used to compare the similarities between the two datasets. The thermal camera system was programmed with a 30C lower limit to remove irrelevant data points, the system emissivity was set to 1 as a standard for testing. Refer to Appendix L for the C++ code that was used to control the Thermal Camera System.

### 2.5.1 Collected Data

The thermal camera system was used to collect the thermal signatures of a toaster oven over a set interval of time at 250C and 350C. For the demonstration, 250C will be set as the nominal operation value of the toaster oven and 350C will be set as the aberrant operation value. Refer to Figure 9 for a scatter plot of the collected data.

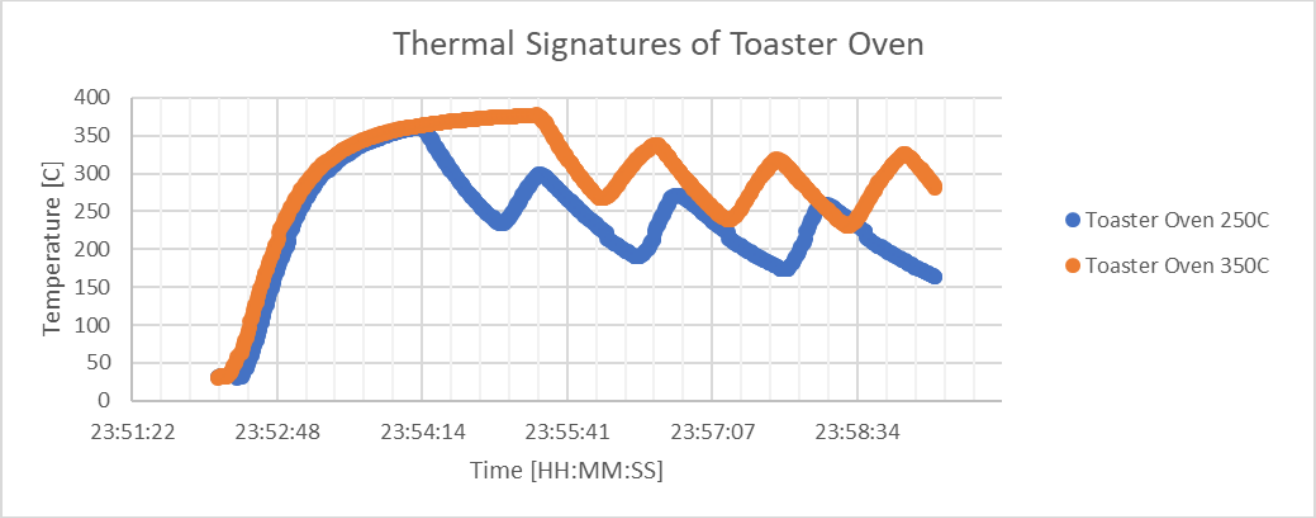


*Figure 9: Thermal Signatures of Toaster Oven at 350C and 250C Settings*

### 2.5.2 Created Metrics

It should be noted that several metrics could be used to analyze the two signatures, these two metrics are used because of their previous application within the Electrical Engineering Technology program. The two metrics used to assess the variability of the nominal and aberrant signatures are Pearson's Correlation Coefficients and definite integrals. When both metrics are used and compared a qualified Technologist can make an accurate prediction of the operational status of the monitored equipment; further, tolerance setpoints can be deduced from the analysis and programmed into the monitoring system for specific apparatus.

#### *2.5.2.1 Pearson's Correlation Coefficient*

Pearson's coefficient is a calculation that measures the strength of the linear relationship between two variables [32]. Pearson's coefficient is defined as

$$r = \frac{n\Sigma(xy) - (\Sigma x)(\Sigma y)}{\sqrt{[n\Sigma x^2 - (\Sigma x)^2][n\Sigma y^2 - (\Sigma y)^2]}}$$

[31]

The value and polarity of $r$ describes the correlation strength and proportionality, respectively [32]. Where strength is $-1 \leq r \geq 1$ with greater relational strength near $\pm 1$, and proportionality is direct when positive and inverse when negative [32].

The collected data was used to calculate Pearson's Coefficient with 250C temperature data as x and 350C temperature data as y. This resulted with an $r = +0.792146428$, this shows a strong positive relationship but as Figure 9 shows the toaster oven initially heats very similarly at operational or aberrant temperatures which skew the function to see more of a linear relationship. The Pearson's Coefficient was recalculated from 23:54:14 to 23:59:20, this resulted with $r = +0.44572$, this shows a correlation much less than the initial calculation and is more representational of the difference between the two datasets.

*2.5.2.2 Definite Integral*

Integrals evaluate the area under a function or curve. The EET program extensively uses integrals, and integrals were previously used in this report to derive Stefan-Boltzmann's law from Planck's Equation. Here the integral is used to solve

$$F(t) = \int_{start}^{end} f(t)\, dt$$

the integral can be computed easily because of the discrete data collected. Each temperature data point has 0.5s duration; therefore, the area under the curves is approximated by the sum of the discrete areas calculated as

$$F(t) = \sum (T_n * t_n)$$

Because the integral does not relate the two datasets each temperature dataset was calculated separately and then similarity and difference percentages were calculated to compare the calculations. $F(250C) = 95189.51355Cs$ and $F(350C) = 116121.2289Cs$ with $F(250C)$ as a base the similarity and difference are 121.99% and 21.99%, respectively. The integrals were recalculated to omit the

common heating sections of data to remain consistent with the Pearson's calculations. The integral percentages will not change significantly because the area under the curve is virtually equal for both temperatures when heating. The recalculation showed $(250C) = 66990.5105Cs$ and $F(350C) = 86288.2175Cs$ with $F(250C)$ as a base, the similarity and difference are 128.81% and 28.81%, respectively.

#### *2.5.2.3 Metric Interpretation*

The Pearson's coefficients and integrals can be used together to interpret the degree of deviation from operational conditions and allow for the categorization of aberrant conditions. For the data analysis with the initial heating period omitted the $r = +0.44572$ and integral difference of +28.81%. This information shows that over the same period of time a larger amount of energy was used to heat the toaster oven based on the +28.81% integral difference and that the linear correlation between temperature points is directly proportional but not strongly linked based on the low positive Pearson's correlation coefficient.

If a nominal tolerance for the toaster oven must be within 10% of nominal operation, then the Pearson's correlation coefficient should be greater than ±0.90 and the integral for the interval should be within $60291.4595Cs\ to\ 73689.5615Cs$. The actual average temperature of the toaster oven was 237.61C and 294.88C for 250C and 350C settings, respectively. The difference of average temperature was 24.10% from nominal, this value is directly related to the integral difference of 28.81% and further corroborates the aberrant toaster oven condition. These values can be used as the categorization of aberrant operation of the toaster oven; where, values of temperature that exceed both tolerances would indicate aberrant conditions and the monitoring system would output an alarm signal.

### 2.5.3 Industry Applications

The proposed thermal camera system could be installed to monitor rotating machines, splices, high load fuses, 3 phase imbalances in panels, arc-flash potential areas, apparatus oil levels, and any

application where radiated heat records can be useful. There are many applications that heat signatures have because of the relationships between heat, as a power loss, and current and voltage.

### 2.5.4 Advanced Data Analysis

Advanced data analysis methods such as artificial neural networks for data classification [34], load current influence on temperature [35], and partial discharge detection [36] are examples of where the investigation should continue for the proposed thermal camera system.

# 3.0 Conclusions

1. All electrical systems produce power losses in the form of heat which can damage the system apparatus.
2. All objects above zero kelvin radiate infrared spectrum energy.
3. All infrared radiation can be detected with an infrared detector.
4. A thermal camera system can be used to monitor and log equipment temperature.
5. Apparatus temperature can be analyzed to create metrics for proper and aberrant operation.
6. Equipment temperature metrics can be used as benchmarks for system health; primarily, to determine the proper and aberrant operation of apparatus.
7. Advanced metrics can be used for sophisticated system/apparatus health.

# 4.0 Recommendations

1. Determine a list of suspect apparatus.
2. Begin monitoring suspect apparatus with the thermal camera system.
3. Create metrics for proper and aberrant operation of apparatus.
4. Set alarms for apparatus that surpass the tolerance limits of the metrics.
5. Investigate applications for advanced data analysis metrics and system-wide nodal analysis metrics.

# 5.0 Appendix

## 5.1 Appendix A: Historical Timeline of Infrared Detection Advancements

| Year | Event |
|---|---|
| 1800 | Discovery of the existence of thermal radiation in the invisible beyond the red by W. HERSCHEL |
| 1822 | Discovery of the thermoelectric effects using an antimony–copper pair by T. J. SEEBECK |
| 1830 | Thermal element for thermal radiation measurement by L. NOBILI |
| 1833 | Thermopile consisting of 10 in-line Sb-Bi thermal pairs by L. NOBILI and M. MELLONI |
| 1834 | Discovery of the PELTIER effect on a current-fed pair of two different conductors by J. C. PELTIER |
| 1835 | Formulation of the hypothesis that light and electromagnetic radiation are of the same nature by A. M. AMPÈRE |
| 1839 | Solar absorption spectrum of the atmosphere and the role of water vapour by M. MELLONI |
| 1840 | Discovery of the three atmospheric windows by J. HERSCHEL (son of W. HERSCHEL) |
| 1857 | Harmonisation of the three thermoelectric effects (SEEBECK, PELTIER, THOMSON) by W. THOMSON (Lord KELVIN) |
| 1859 | Relationship between absorption and emission by G. KIRCHHOFF |
| 1864 | Theory of electromagnetic radiation by J. C. MAXWELL |
| 1879 | Empirical relationship between radiation intensity and temperature of a blackbody by J. STEFAN |
| 1880 | Study of absorption characteristics of the atmosphere through a Pt Bolometer resistance by S. P. LANGLEY |
| 1883 | Study of transmission characteristics of IR-transparent materials by M. MELLONI |
| 1884 | Thermodynamic derivation of the STEFAN law by L. BOLTZMANN |
| 1894, 1900 | Derivation of the wavelength relation of blackbody radiation by J. W. RAYEIGH and W. WIEN |
| 1903 | Temperature measurements of stars and planets using IR radiometry and spectrometry by W. W. COBLENTZ |
| 1914 | Application of bolometers for the remote exploration of people and aircrafts |
| 1930 | IR direction finders based on PbS quantum detectors in the wavelength range 1.5–3.0 µm for military applications (GUDDEN, GÖRLICH and KUTSCHER), increased range in World War II to 30 km for ships and 7 km for tanks (3–5 µm) |
| 1934 | First IR image converter |
| 1939 | Development of the first IR display unit in the US (Sniperscope, Snooperscope) |
| 1947 | Pneumatically acting, high-detectivity radiation detector by M.J.E. GOLAY |
| 1954 | First imaging cameras based on thermopiles (exposure time of 20 min per image) and on bolometers (4 min) |
| 1955 | Mass production start of IR seeker heads for IR guided rockets in the US (PbS and PbTe detectors, later Sb detectors for Sidewinder rockets) |
| 1965 | Mass production start of IR cameras for civil applications in Sweden (single-element sensors with optomechanical scanner: AGA Thermografiesystem 660) |
| 1968 | Production start of IR sensor arrays (monolithic Si-arrays: R.A. SOREF 1968; IR-CCD: 1970; SCHOTTKY diode arrays: F.D. SHEPHERD and A.C. YANG 1973; IR-CMOS: 1980; SPRITE: T. ELIOTT 1981) |
| 1995 | Production start of IR cameras with uncooled FPAs (Focal Plane Arrays; microbolometer-based and pyroelectric) |

[8]

## 5.2 Appendix B: Integral of Planck's Law

$$Integral\ of\ \frac{I}{A} = \int_0^{\infty} I(\lambda)\, d\lambda = \frac{2\pi hc^2}{\lambda^5} * \frac{1}{e^{\left(\frac{hc}{k\lambda T}\right)} - 1} d\lambda = \frac{2\pi^5 k^4}{15c^2k^3} T^4 = \sigma T^4$$

[8]

## 5.3 Appendix C: Derivative of Planck's Law

$$A = \frac{hc}{kT} \therefore \frac{dI(\lambda)}{d\lambda} = \left(2\pi ckT \frac{A}{\lambda^5} * \frac{1}{e^{\frac{A}{\lambda}} - 1}\right)' = \left(\frac{1}{\lambda^5} * \frac{1}{e^{\frac{A}{\lambda}} - 1}\right)' = (uv)'$$

Product rule to evaluate derivative.

$$(uv)' = u'v + uv'$$

$$(u)' = \left(\frac{1}{\lambda^5}\right)' = -\frac{5}{\lambda^6}$$

$$(v)' = \left(\frac{1}{e^{\frac{A}{\lambda}} - 1}\right)' = \frac{A}{\lambda^2} * \frac{e^{\frac{A}{\lambda}}}{\left(e^{\frac{A}{\lambda}} - 1\right)^2}$$

$$(uv)' = -\frac{5}{\lambda^6}\frac{1}{e^{\frac{A}{\lambda}} - 1} + \frac{1}{\lambda^5}\frac{A}{\lambda^2} * \frac{e^{\frac{A}{\lambda}}}{\left(e^{\frac{A}{\lambda}} - 1\right)^2} = 0$$

Insert A in again and simplify.

$$\frac{hc}{\lambda kT}\frac{1}{1 - e^{-\frac{hc}{\lambda kT}}} - 5 = 0$$

Substitute x into eq. and simplify.

$$x = \frac{hc}{\lambda kT}\ into\ \frac{hc}{\lambda kT}\frac{1}{1 - e^{-\frac{hc}{\lambda kT}}} - 5 = 0$$

$$\frac{x}{1 - e^{-x}} = 5 \therefore (x - 5)e^x = -5$$

Expand by $e^{-5}$;

$$(x - 5)e^{x-5} = -5e^{-5}$$

Using Lambert W function.

$$\boldsymbol{W\left((x-5)e^{x-5}\right) = W\left(-5e^{-5}\right)}$$

$$x = 5 + W(-5e^{-5}) = 4.96511$$

Substitute X into Equation.

$$4.96511 = \frac{6.626x10^{-34} * 2.997x10^8}{\lambda T 1.38x10^{-23}}$$

$$\lambda(T) = \frac{2.898x10^{-3} Km}{T}$$

$$\lambda T = 2.898K\mu m$$

[8]

## 5.4 Appendix D: Example of Electrical and Blackbody Radiation Formulas

$$P = \sigma A T^4 \ \& \ P = I^2 R$$

$$\therefore$$

$$\sigma A T^4 = I^2 R$$

$$\therefore$$

$$I = \sqrt{\frac{\sigma A T^4}{R}}$$

## 5.5 Appendix E: List of Detector Types and Methods of Operation

| Detector | Method of Operation |
|---|---|
| Bolometer<br>Metal<br>Semiconductor<br>Superconductor<br>Ferroelectric<br>Hot electron | Change in electrical conductivity |
| Thermocouple/thermopile | Voltage generation, caused by change in temperature of the junction of two dissimilar materials |
| Pyroelectric | Changes in spontaneous electrical polarization |
| Golay cell/gas microphone | Thermal expansion of a gas |
| Absorption edge | Optical transmission of a semiconductor |
| Pyromagnetic | Changes in magnetic properties |
| Liquid crystal | Changes of optical properties |

[3]

## 5.6 Appendix F: Thermopile Array MLX90640 Array Readout

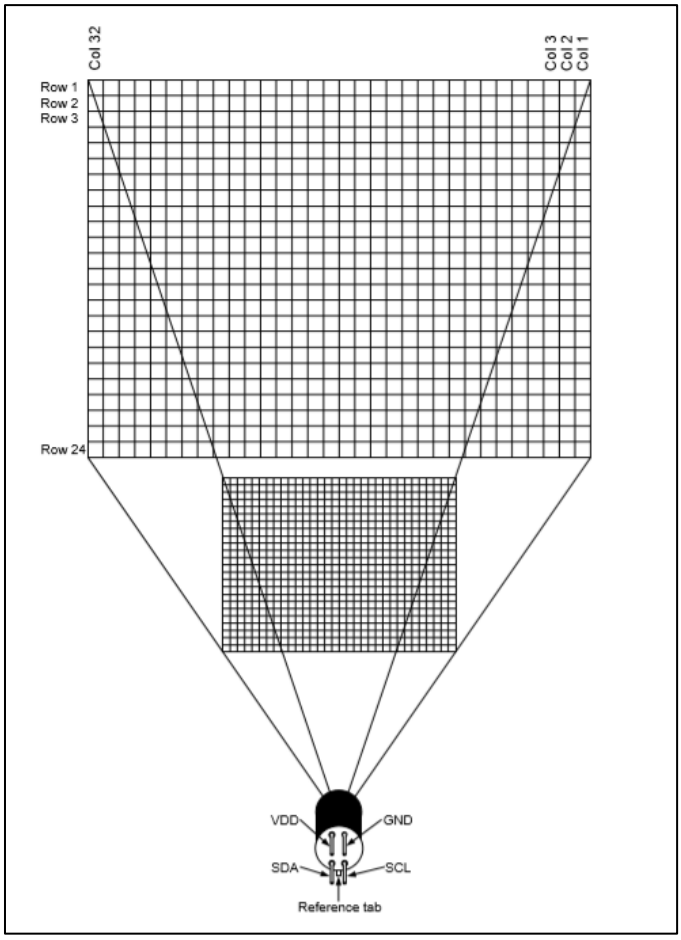


[21]

## 5.7 Appendix G: S.P. Langley Bolometer Diagram

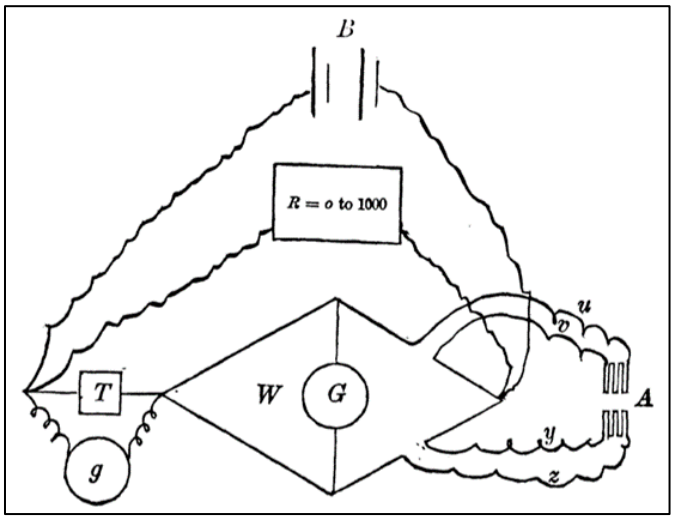


[6]

## 5.8 Appendix H: Micro-Bolometer Schematic and Cut through

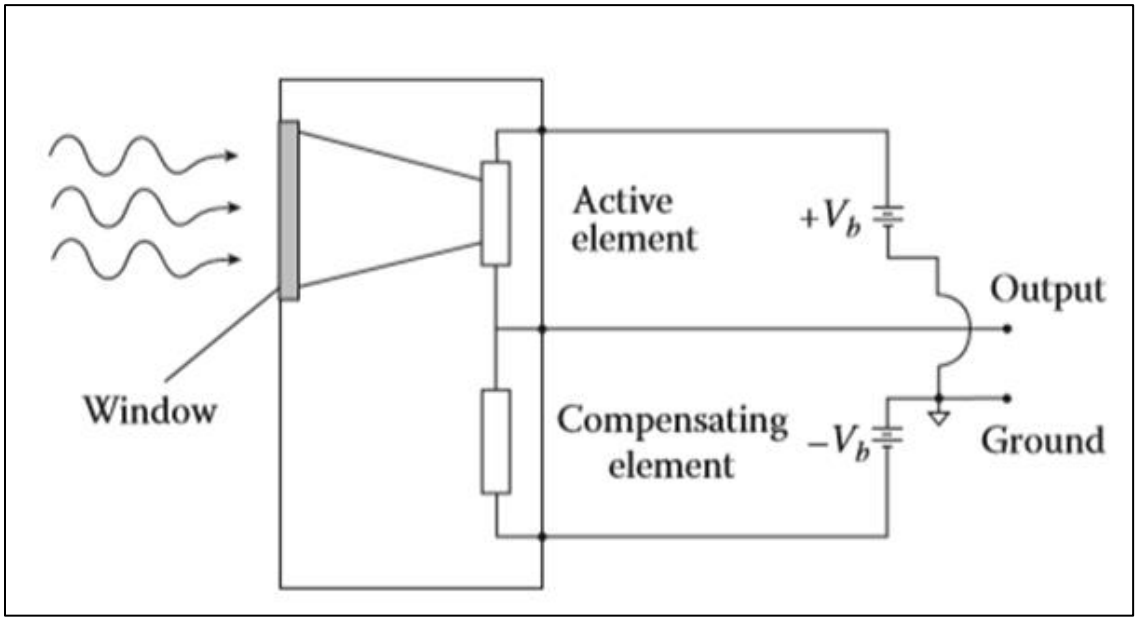


[3]

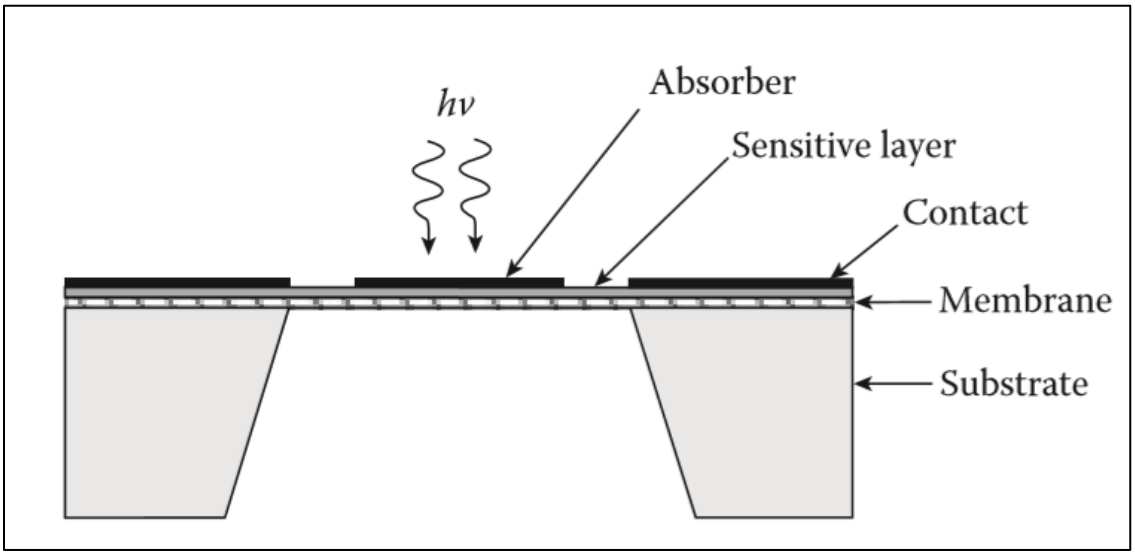


[3]

## 5.9 Appendix I: Transmittance Table of Optical Materials

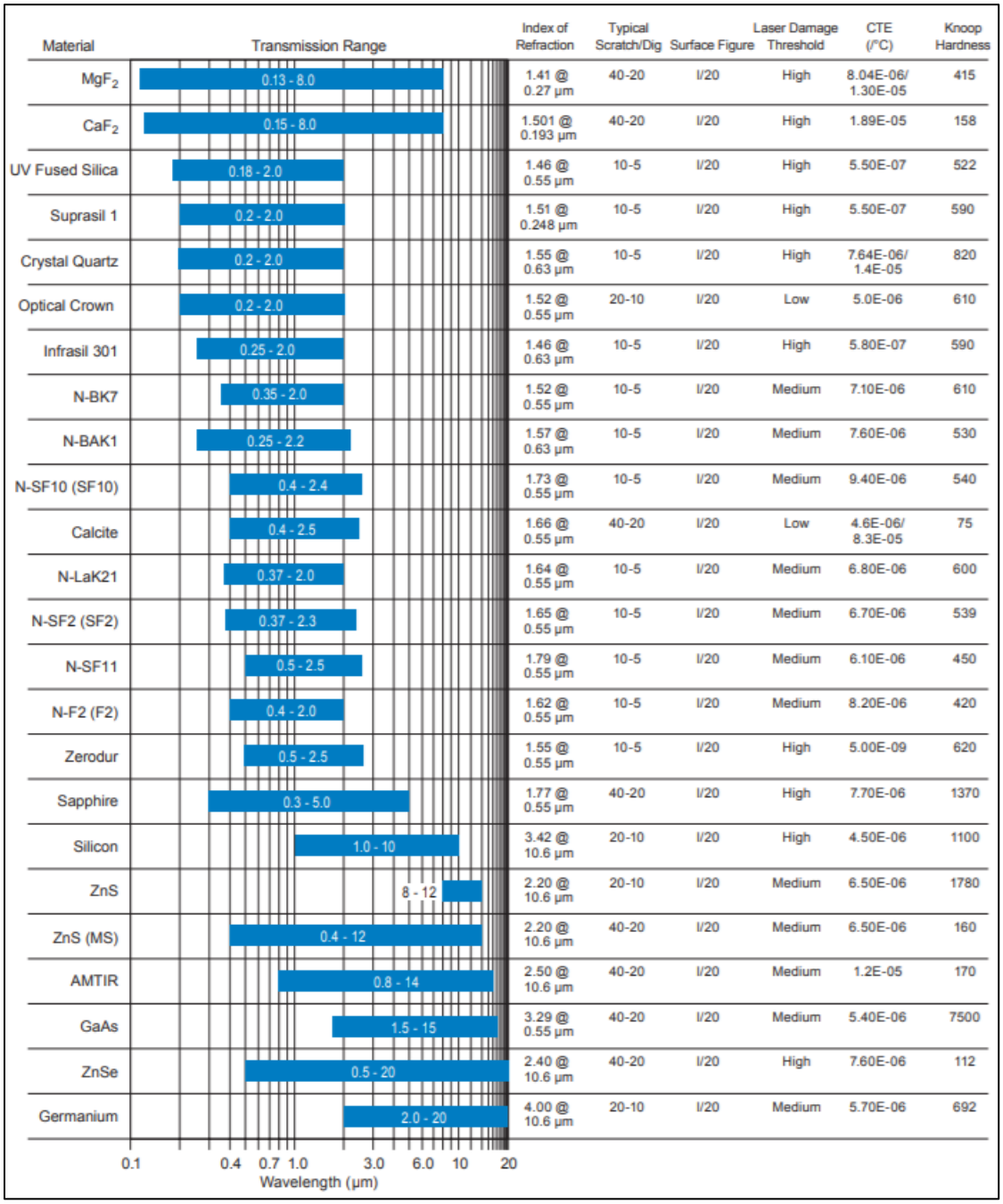


[14]

## 5.10 Appendix J: Engineering Reliability Work Scope

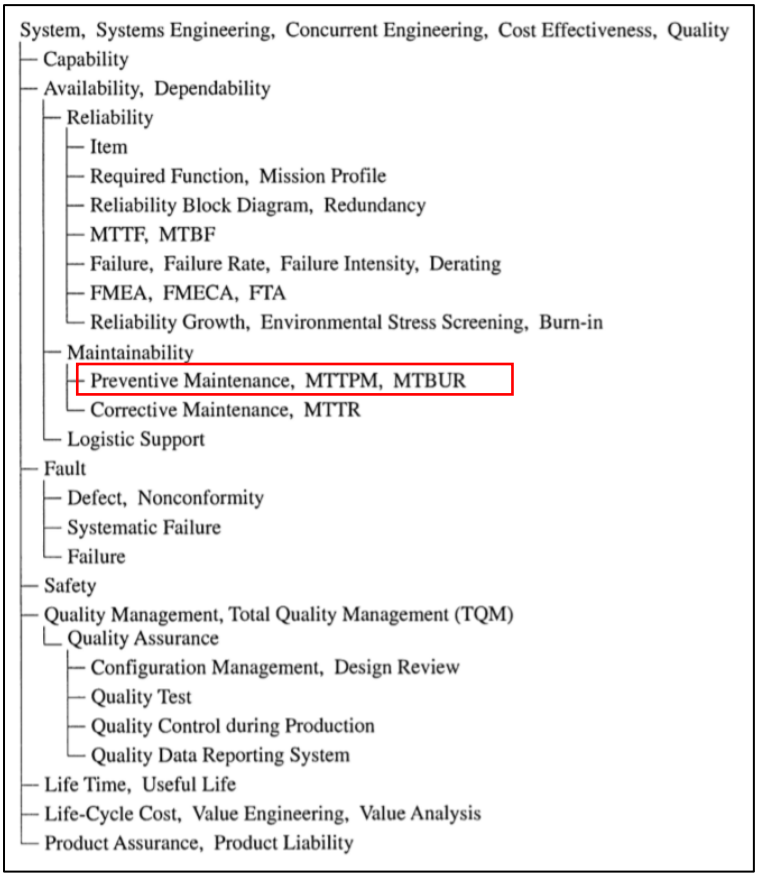


[15]

## 5.11 Appendix K: NETA/ANSI Thermal Inspection Tolerance Table

| Temperature difference (ΔT) based on comparisons between similar components under similar loading. | Temperature difference (ΔT) based upon comparisons between component and ambient air temperatures. | Recommended Action |
|---|---|---|
| 1°C - 3°C | 1°C - 10°C | Possible deficiency; warrants investigation |
| 4°C - 15°C | 11°C - 20°C | Indicates probable deficiency; repair as time permits |
| - - - - - - | 21°C - 40°C | Monitor until corrective measures can be accomplished |
| >15°C | >40°C | Major discrepancy; repair immediately |

Temperature specifications vary depending on the exact type of equipment. Even in the same class of equipment (i.e., cables) there are various temperature ratings. Heating is generally related to the square of the current; therefore, the load current will have a major impact on ΔT. In the absence of consensus standards for ΔT, the values in this table will provide reasonable guidelines.

An alternative method of evaluation is the standards-based temperature rating system as discussed in Chapter 8.9.2, Conducting an IR Thermographic Inspection, *Electrical Power Systems Maintenance and Testing*, by Paul Gill, PE, 1998.

It is a necessary and valid requirement that the person performing the electrical inspection be thoroughly trained and experienced concerning the apparatus and systems being evaluated as well as knowledgeable of thermographic methodology.

[18]

## 5.12 Appendix L: Thermal Camera Sample Code C++

```
#include <stdint.h>
#include <iostream>
#include <cstring>
#include <fstream>
#include <chrono>
#include <thread>
#include <math.h>
#include "headers/MLX90640_API.h"
#include "lib/fb.h"
#include <ctime>

using namespace std;

//Start time for timestamp
string getTimeStr(){
time_t now = std::chrono::system_clock::to_time_t(std::chrono::system_clock::now());

string s(30, '\0');
strftime(&s[0], s.size(), "%Y-%m-%d %H:%M:%S", std::localtime(&now));
return s;
}

//SPI Address for MLX90640
#define MLX_I2C_ADDR 0x33

#define IMAGE_SCALE 5

// Valid frame rates are 1, 2, 4, 8, 16, 32 and 64
// The i2c baudrate is set to 1mhz to support these
#define FPS 2
#define FRAME_TIME_MICROS (1000000/FPS)

// Despite the framerate being ostensibly FPS hz
// The frame is often not ready in time
// This offset is added to the FRAME_TIME_MICROS
// to account for this.
#define OFFSET_MICROS 850


uint8_t font[] = {
0b01111110,
0b10000001,
0b10000001,
0b10000001,
0b01111110,
```

```
0b00000000,
0b00000001,
0b11111111,
0b10000001,
0b00000000,

0b01100001,
0b10010001,
0b10010001,
0b10010001,
0b10001111,

0b01101110,
0b10010001,
0b10010001,
0b10010001,
0b10010001,

0b11111111,
0b00010000,
0b00010000,
0b00010000,
0b11100000,

0b10001111,
0b10010001,
0b10010001,
0b10010001,
0b01100001,

0b10001110,
0b10010001,
0b10010001,
0b10010001,
0b01111110,

0b11111111,
0b10000000,
0b10000000,
0b10000000,
0b10000000,

0b01101110,
0b10010001,
0b10010001,
0b10010001,
0b01101110,
```

```
0b11111111,
0b10010000,
0b10010000,
0b10010000,
0b01100000
};
void put_pixel_scaled(int x, int y, int r, int g, int b){
x *= IMAGE_SCALE;
y *= IMAGE_SCALE;
for (int px = 0; px < IMAGE_SCALE; px++){
for (int py = 0; py < IMAGE_SCALE; py++){
fb_put_pixel(x + px, y + py, r, g, b);
}
}
}
void put_digit(int x, int y, int number) {
for (int n_x = 0; n_x < 5; n_x++) {
int col = font[(number * 5) + (4-n_x)];
for (int n_y = 0; n_y < 8; n_y++) {
int pixel = (col & 0b10000000) ? 255 : 0;
col <<= 1;
put_pixel_scaled(x + n_x, y + n_y, pixel, pixel, pixel);
}
}
}
void put_number(int x, int y, float number) {
float div = 0.01;
unsigned int digits = 1;
unsigned int o_x = 0;
if (number > 999.99){
number = 999.99;
}
while (div <= number / 10) {
digits++;
div *= 10;
}
if (number < 100) {
put_digit(x + o_x, y, 0);
o_x += 6;
}
while (digits > 0) {
put_digit(x + o_x, y, number / div);
number = fmod(number, div);
div /= 10;
if (digits == 3){
put_pixel_scaled(x + o_x + 6, y + 7, 255, 255, 255);
o_x += 2;
}
```

```
digits--;
o_x += 6;
}
}

void put_pixel_false_colour(int x, int y, double v) {
// Heatmap code borrowed from: http://www.andrewnoske.com/wiki/Code_-
_heatmaps_and_color_gradients
const int NUM_COLORS = 7;
static float color[NUM_COLORS][3] = { {0,0,0}, {0,0,1}, {0,1,0}, {1,1,0}, {1,0,0}, {1,0,1}, {1,1,1} };
int idx1, idx2;
float fractBetween = 0;
float vmin = 5.0;
float vmax = 50.0;
float vrange = vmax-vmin;
v -= vmin;
v /= vrange;
if(v <= 0) {idx1=idx2=0;}
else if(v >= 1) {idx1=idx2=NUM_COLORS-1;}
else
{
v *= (NUM_COLORS-1);
idx1 = floor(v);
idx2 = idx1+1;
fractBetween = v - float(idx1);
}

int ir, ig, ib;

ir = (int)((((color[idx2][0] - color[idx1][0]) * fractBetween) + color[idx1][0]) * 255.0);
ig = (int)((((color[idx2][1] - color[idx1][1]) * fractBetween) + color[idx1][1]) * 255.0);
ib = (int)((((color[idx2][2] - color[idx1][2]) * fractBetween) + color[idx1][2]) * 255.0);

put_pixel_scaled(x, y, ir, ig, ib);
/*for(int px = 0; px < IMAGE_SCALE; px++){
for(int py = 0; py < IMAGE_SCALE; py++){
fb_put_pixel(x + px, y + py, ir, ig, ib);
}
}*/
}

int main(){
ofstream myFile;
myFile.open("test.csv");
static uint16_t eeMLX90640[832];
float emissivity = 1;
uint16_t frame[834];
static float image[768];
```

```
static float mlx90640To[768];
float eTa;
static uint16_t data[768*sizeof(float)];

auto frame_time = std::chrono::microseconds(FRAME_TIME_MICROS + OFFSET_MICROS);

MLX90640_SetDeviceMode(MLX_I2C_ADDR, 0);
MLX90640_SetSubPageRepeat(MLX_I2C_ADDR, 0);
switch(FPS){
case 1:
MLX90640_SetRefreshRate(MLX_I2C_ADDR, 0b001);
break;
case 2:
MLX90640_SetRefreshRate(MLX_I2C_ADDR, 0b010);
break;
case 4:
MLX90640_SetRefreshRate(MLX_I2C_ADDR, 0b011);
break;
case 8:
MLX90640_SetRefreshRate(MLX_I2C_ADDR, 0b100);
break;
case 16:
MLX90640_SetRefreshRate(MLX_I2C_ADDR, 0b101);
break;
case 32:
MLX90640_SetRefreshRate(MLX_I2C_ADDR, 0b110);
break;
case 64:
MLX90640_SetRefreshRate(MLX_I2C_ADDR, 0b111);
break;
default:
printf("Unsupported framerate: %d", FPS);
return 1;
}
MLX90640_SetChessMode(MLX_I2C_ADDR);

paramsMLX90640 mlx90640;
MLX90640_DumpEE(MLX_I2C_ADDR, eeMLX90640);
MLX90640_ExtractParameters(eeMLX90640, &mlx90640);

fb_init();

while (1){
float hotspot = 0;
int hotspot_x = 0;
int hotspot_y = 0;
auto start = std::chrono::system_clock::now();
```

```
MLX90640_GetFrameData(MLX_I2C_ADDR, frame);
// MLX90640_InterpolateOutliers(frame, eeMLX90640);

eTa = MLX90640_GetTa(frame, &mlx90640);
MLX90640_CalculateTo(frame, &mlx90640, emissivity, eTa, mlx90640To);

MLX90640_BadPixelsCorrection((&mlx90640)->brokenPixels, mlx90640To, 1, &mlx90640);
MLX90640_BadPixelsCorrection((&mlx90640)->outlierPixels, mlx90640To, 1, &mlx90640);

for(int y = 0; y < 24; y++){
for(int x = 0; x < 32; x++){
float val = mlx90640To[32 * (23-y) + x];
if (val > hotspot){
hotspot = val;
hotspot_x = y;
hotspot_y = x;
}
put_pixel_false_colour(y, x, val);
}
}

if (hotspot > 30){
myFile << hotspot << "," << "C" << "," << getTimeStr() << endl;
}
if(hotspot_x - 1 >= 0){
put_pixel_scaled(hotspot_x - 1, hotspot_y, 255, 255, 255);
}
if(hotspot_x + 1 < 24){
put_pixel_scaled(hotspot_x + 1, hotspot_y, 255, 255, 255);
}
if(hotspot_y - 1 >= 0){
put_pixel_scaled(hotspot_x, hotspot_y - 1, 255, 255, 255);
}
if(hotspot_y + 1 < 32){
put_pixel_scaled(hotspot_x, hotspot_y + 1, 255, 255, 255);
}
put_number(0, 33, hotspot);


auto end = std::chrono::system_clock::now();
auto elapsed = std::chrono::duration_cast<std::chrono::microseconds>(end - start);
std::this_thread::sleep_for(std::chrono::microseconds(frame_time - elapsed));

}

return 0;
}
```

# 6.0 References


[1] W. Herschel, “Experiments on the Solar, and on the Terrestrial Rays that Occasion Heat; With a Comparative View of the Laws to Which Light and Heat, or Rather the Rays Which Occasion Them, are Subject, in Order to Determine Whether They are the Same, or Different. Part I. By William Herschel, LL. D. F. R. S.”, Phil. Trans. of the Royal Soc. of Lond., Vol. 90, pp. 293-326, 1800.

[2] W. Herschel, “Experiments on the Solar, and on the Terrestrial Rays that Occasion Heat; With a Comparative View of the Laws to Which Light and Heat, or Rather the Rays Which Occasion Them, are Subject, in Order to Determine Whether They are the Same, or Different. Part II. By William Herschel, LL. D. F. R. S.”, Phil. Trans. of the Royal Soc. of Lond., Vol. 90, pp. 437-538, 1800.

[3] A. Rogalski, “Thermal Detectors”, 2nd ed. Boca Raton: CRC Press, 2011.

[4] M. Vollmer and K.P. Möllman, “Infrared Thermal Imaging”, 2nd ed. Germany: Wiley-VCH, 2018.

[5] E. Colombi, “Macedonio Melloni between physics and political commitment” Il. Nuo. Cimen., vol. 37 C, no. 4, pp. 285-303, 2014.

[6] S.P. Langley, “The Bolometer and Radiant Energy”, Amer. Acad. Of Arts and Sci., Vol. 16, pp. 342-358, 1881.

[7] M. Planck, “On the Law of Distribution of Energy in the Normal Spectrum”, Ann. der Phys., vol. 4, pp. 553, 1901.

[8] H. Budzier and G. Gerlach, “Thermal Infrared Sensors Theory, Optimization and Practice,” 1st ed. West Sussex, U.K.: John Wiley & Sons, 2011.

[9] R. L. Boylestad, “Introductory Circuit Analysis,” 13th ed. Boston: Pearson, 2016.

[10] S. Abdan, N. Stosic, A. Kovacevic, I. Smith and N. Asati, “Analysis of rolling bearing power loss models for twin screw oil injected compressor,” in IOP Conf. Seri: Mat. Sci. and Eng.: IOP Publishing, 2019, pp 1-10.

[11] Y. Yoshikuni and M. Ryuji, “Estimating Power Outage Costs Based on a Survey of Industrial Customers,” *Elect. Eng. Jpn., vol. 185, no. 4, pp. 25-32, Aug, 2013.*

[12] “Melexis Far Infrared Thermal Sensor MLX90640.” Research and Markets. https://bit.ly/3cfqjf6 (accessed Apr. 14, 2020)

[13] E. Hecht, “Optics,” 4th ed. San Francisco: Pearson, 2002.

[14] Material Properties, 1st ed. IDEX, Albuquerque, NM.

[15] A. Birolini, “Reliability Engineering Theory and Practice”, 6th ed. Tuscany, Italy: Springer, 2010.

[16] National Aeronautics and Space Administration, *Reliability-Centered Maintenance Guide for Facilities and Collateral Equipment,* Final, 2008.

[17] Department of the Army, *Failure Modes, Effects and Criticality Analyses (FMECA) for Command, Control, Communications, Computer, Intelligence, Surveillance, and Reconnaissance (C4ISR) Facilities*, TM 5-698-4, 2006.

[18] Standard of Acceptance Testing Specifications for Electrical Power Equipment and Systems, ANSI/NETA ATS-2017, 2017.

[19] *Aluminum Electrical Conductor Handbook,* the Aluminum Association, Washington, 1989. pp. 2.1-2.3.

[20] Raspberry Pi Foundation, “Raspberry Pi 3 Model B+” datasheet.

[21] Melexis, “MLX90640 32X24 IR array” MLX90640 datasheet, Jun. 2016 [Revised Dec. 2019].

[22] E. Naramore, J. Gerner, Y. L. Scouarnec, J. Stolz, and M. K. Glass, “Beginning PHP5, Apache, MySQL Web Development”, 1st ed. Indianapolis: Wiley, 2005.

[23] B. Laurie and P. Laurie, “Apache: The Definitive Guide”, 3rd ed. Sebastopol: O’Riely Media, 2002.

[24] “Comparison of web server software.” Wikipedia. https://en.wikipedia.org/wiki/ Comparison_of_web _server_software (accessed Apr. 10, 2020)

[25] “MySQL Customers.” MySQL. https://www.mysql.com/customers/ (accessed Apr. 10, 2020)

[26] “MLX90640 Sensor.” Pimoroni Shop. https://shop.pimoroni.com/products/mlx90640-thermal-camera-breakout?variant=12549161746515 (accessed Apr. 14, 2020)

[27] “Raspberry Pi Zero W.” Pimoroni Shop. https://shop.pimoroni.com/products/raspberry-pi-zero-w (accessed Apr. 14, 2020)

[28] “PiTFT 240x240 Display.” Pimoroni Shop. https://shop.pimoroni.com/products/adafruit-mini-pitft-1-3-240x240-tft-add-on-for-raspberry-pi (accessed Apr. 14, 2020)

[29] “MLX90640ESF-BAA-000-TU.” Digi-key Shop. https://www.digikey.ca/en/products/detail/ melexis-technologies-nv/MLX90640ESF-BAA-000-TU/8638463 (accessed Apr. 14, 2020)

[30] “104990542.” Digi-key Shop. https://www.digikey.ca/product-detail/en/seeed-technology-co-ltd/104990542/1597-104990542-ND/10244653 (accessed Apr. 14, 2020)

[31] “FLIR Science Camera Rental Program.” FLIR. https://www.flir.ca/instruments/science/rdrental/ (accessed Apr. 14, 2020)

[32] B. Illowsky and S. Dean, “Introductory Statistics”, 1st ed. Houston, Texas: OpenStax, 2013.

[33] Majka, Marcin & Majka, Tomasz. (2013). Healthy Light Source. 10.3390/wsf2-00933.

[34] F. Al-Obaidy, “IC TESTING USING THERMAL IMAGE BASED ON INTELLIGENT CLASSIFICATION METHODS,” MASc thesis, Ryerson University, Toronto, 2016.

[35] E. Bortoni, L. Santos, G. Bastos, L. Souza, and M. Craveiro, “Extracting Load Current Influence From Infrared Thermal Inspections,” IEEE Trans. Power Del., vol. 26, no. 2, pp. 501-505, 2011.

[36] A. Gonzalez-Parada, R. Guzman-Cabrera, M. Torres-Cisneros, and J. R. Guzman-Sepulveda, “Comparative Analysis of Thermography Studies and Electrical Measurement of Partial Discharges in Underground Power Cables,” Int. J. Thermo., vol. 26, pp 2356-2369, 2015, doi: 10.1007/S10765-015-1926-Z.